Construction and Building Materials 496 (2025) 143759

Contents lists available at ScienceDirect

Construction and Building Materials

journal homepage: www.elsevier.com/locate/conbuildmat

Performance and implications of cost-effective natural sand substitutes for quartz in ultra-high performance concrete

Zhengye Tang [a], Min-Chun Han [a], Sherif El-Tawil [a], Sukhoon Pyo [a,b,*]

[a] Department of Civil & Environmental Engineering, University of Michigan, 2350 Hayward, G.G. Brown, Ann Arbor, MI 48109-2125, USA
[b] Department of Civil, Urban, Earth, and Environmental Engineering, Ulsan National Institute of Science and Technology (UNIST), 50 UNIST-gil, Ulju-gun, Ulsan 44919, Republic of Korea

ARTICLE INFO

Keywords:
Ultra-high performance concrete (UHPC)
Economical UHPC
Sand type
Tensile behavior

ABSTRACT

This study experimentally investigated the use of locally available natural sands as cost-effective substitutes for high-purity quartz sand in ultra-high performance concrete (UHPC). Motivated by the low cost of natural sands, which can be up to 95 % less expensive than quartz sand, four regional sand types (mason, golf, desert, and bunker sand) were evaluated as full or partial replacements. The experimental program assessed the impact of sand selection on particle packing efficiency, fresh workability, compressive strength, fiber pull-out behavior, and composite-scale tensile performance. All alternative sands produced UHPCs with compressive strengths exceeding 150 MPa, with some partial replacements outperforming the reference silica sand mixture. Single-fiber pull-out tests of smooth and striated steel fibers demonstrated that aggregate morphology, particularly angularity and surface texture, substantially enhances the fiber–matrix interfacial bond, with the most pronounced effects observed in bunker and desert sand systems. This improvement led to increased tensile strength and strain-hardening capacity. Additionally, this study demonstrates for the first time the positive effects of sand morphology on the interfacial bond performance of striated steel fibers. These findings indicate that properly selected and proportioned natural sands can reliably replace or supplement quartz sand in UHPC without sacrificing fresh properties or mechanical performance, providing a practical pathway to more cost-effective and sustainable UHPC formulations utilizing abundant regional fine aggregates.

1. Introduction and motivation

Ultra-high performance concrete (UHPC) is a cementitious composite with exceptional mechanical and durability properties, including compressive strength exceeding 150 MPa [23], strain-hardening tensile behavior [2], and high resistance to impact and abrasion [18]. These characteristics are primarily achieved through a synergistic design approach involving a low water-to-binder ratio, highly efficient particle packing, and the use of fine reactive powders and high-range water-reducing admixtures (HRWRs). Among the granular constituents, fine quartz sand, typically well-graded and angular, plays a critical role in establishing a dense matrix that supports the material's mechanical performance and durability.

Quartz sand, also referred to as silica sand, accounts for more than a quarter of UHPC's raw material cost [7] and poses significant sustainability challenges. Quartz sand is not uniformly available across regions, and its production involves energy-intensive processes, including mining, washing, and long-distance transportation, that carry significant environmental impacts and contribute to its high cost. As UHPC adoption expands from specialized to mainstream structural applications, addressing the cost and environmental impacts of quartz sand becomes critical [9].

To address the limitations of quartz sand, there is growing interest in identifying alternative fine aggregates that can partially or fully replace it in UHPC. Previous studies have explored manufactured sands (e.g., crushed sand), recycled fine aggregates, and industrial byproducts, as potential substitutes [15,25,5]. These alternatives differ in mineralogy, particle shape, surface texture, and size distribution, all of which significantly affect packing density, rheology, and fiber–matrix interactions. For instance, Yang et al. [25] emphasized the need for careful grading of manufactured sand to preserve UHPC's strength and flowability, while Li et al. [15] showed that well-blended local sands, when

* Corresponding author at: Department of Civil & Environmental Engineering, University of Michigan, 2350 Hayward, G.G. Brown, Ann Arbor, MI 48109-2125, USA.
E-mail addresses: shpyo@umich.edu, shpyo@unist.ac.kr (S. Pyo).

https://doi.org/10.1016/j.conbuildmat.2025.143759
Received 31 July 2025; Received in revised form 9 September 2025; Accepted 23 September 2025
Available online 26 September 2025

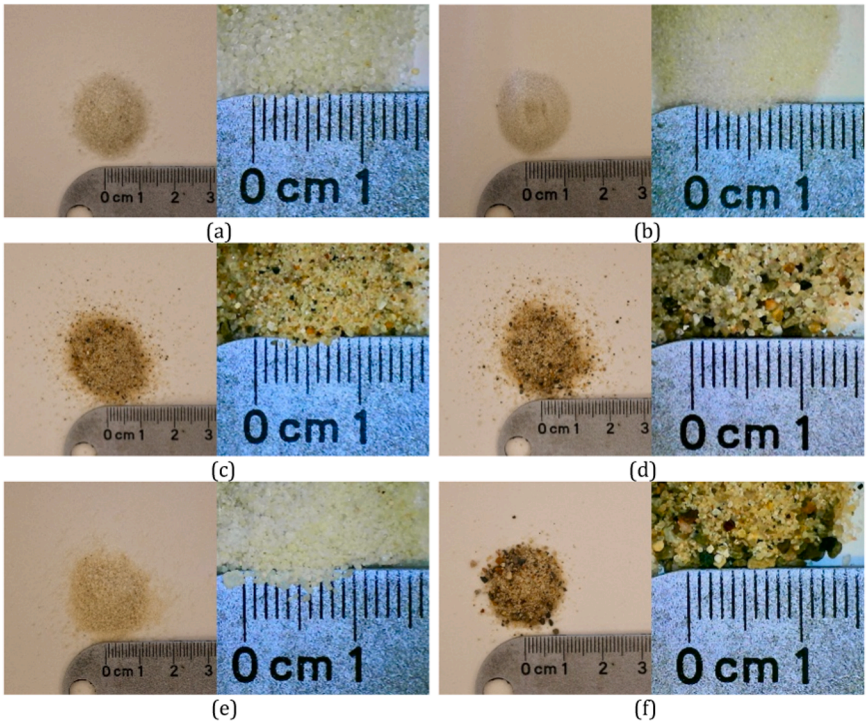

Fig. 1. Particle shape of the sands: (a) F12 Silica sand; (b) F75 Silica sand; (c) Mason sand; (d) Golf sand; (e) Desert sand; (f) Bunker sand.

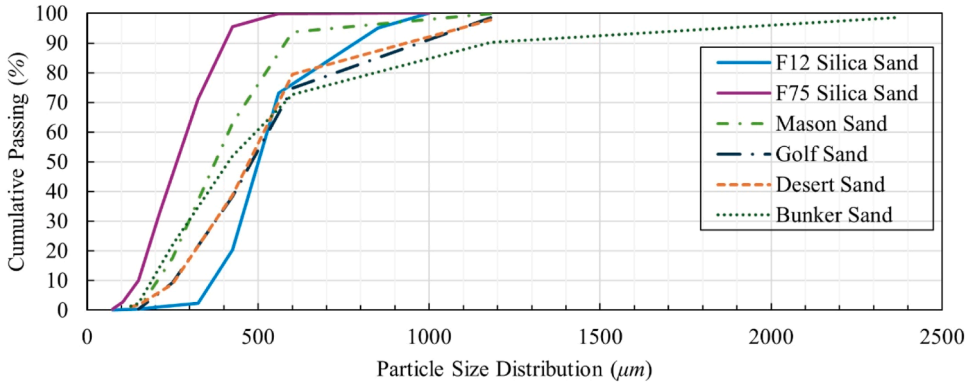

Fig. 2. Particle size distributions of fine aggregates.

combined with ultrafine fillers, could deliver acceptable performance. Kang et al. [13,12] further reported that incorporating steel slag aggregates, owing to their high iron content, can impart self-sensing capabilities to UHPC. Despite these advances, most prior research has focused on manufactured, recycled, or byproduct-derived sands, with limited attention given to systematically evaluating regionally sourced natural sands. This study addresses that gap by investigating the influence of natural sand morphology on UHPC performance and by introducing striated steel fibers to clarify the role of fiber–matrix bonding in tensile resistance.

To address this gap and expand the current knowledge base, this study evaluates the use of four regionally available sands (mason sand, golf sand, desert sand, and bunker sand), as full or partial substitutes for quartz sand in UHPC. These sands are categorized as natural sands because they are sourced directly from naturally occurring geological deposits and undergo only minimal processing, such as washing or screening, unlike manufactured sands, which are produced by crushing rock. As a result, they are both considerably less expensive and have a lower environmental footprint compared to manufactured alternatives. The selected sands encompass a broad range of particle size distributions, mineralogical compositions, and surface textures. Most importantly, they are much more affordable, up to 95 % less costly in some cases than quartz sand, making them highly promising candidates for reducing the overall cost of UHPC. Their successful integration will not only lower material expenses but also facilitate the broader, more sustainable adoption of UHPC in structural applications.

A particle packing analysis was first conducted to evaluate the candidate sands' efficiency in forming a dense granular skeleton. The experimental program included workability assessment, compressive strength testing, single-fiber pull-out tests, and direct tension tests to explore how each sand affects both matrix behavior and fiber–matrix interactions. Particular attention was given to how fiber pull-out response correlates with tensile behavior at the composite level. Previous research has established that while compressive strength in UHPC is largely governed by packing density and matrix homogeneity, tensile properties depend more heavily on the bond strength and energy absorption between fibers and the matrix [20,24]. This distinction underlines the importance of understanding not only the granular skeleton

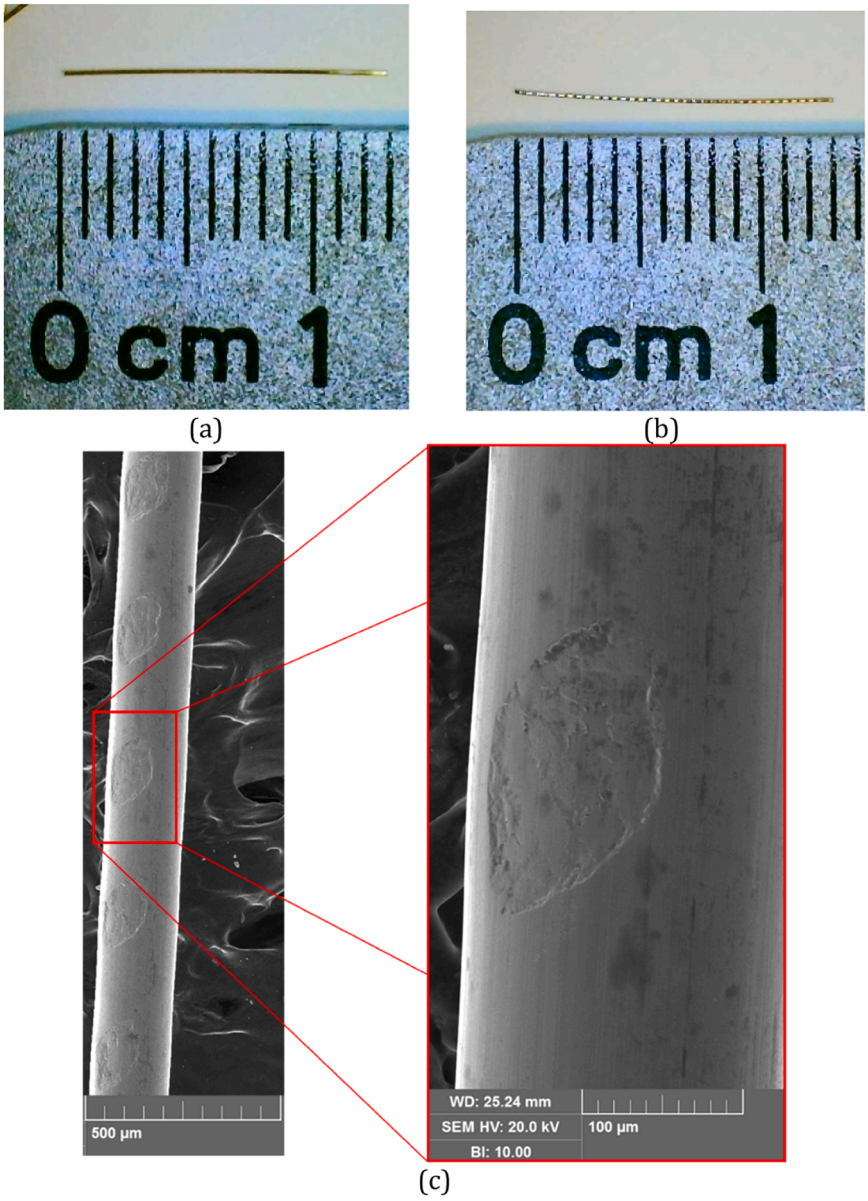

Fig. 3. Steel fiber details: (a) Straight smooth fiber; (b) Striated fiber; (c) SEM image of striated fiber.

but also the interfacial mechanics affected by sand morphology.

2. Experimental program

2.1. Raw materials

An open-source UHPC mixture developed by [8] was adopted for this study. Chosen for both economy and performance, the mix costs only a small fraction of proprietary UHPC formulations and is made from off-the-shelf and commonly available components. The binder system consisted of Type IL cement (MM Concrete, USA), Grade 100 ground-granulated blast-furnace slag (GGBS) (St. Marys, USA), and undensified silica fume (Norchem, USA). A polycarboxylate-based high-range water-reducing admixture (Viscocrete 2100, Sika) was used to ensure adequate flowability.

Five types of fine aggregates were investigated in this study: mason sand, golf sand, bunker sand, desert sand, and two sizes of quartz (silica) sand. Mason sand is a fine aggregate that typically conforms to ASTM C144 or ASTM C33, with a particle size distribution suitable for masonry and plastering work. It is generally sourced from rivers or crushed rock. Golf sand, used for golf course topdressing, is required to meet United States Golf Association (USGA) specifications, which emphasize cleanliness, specific particle size distribution, and a low content of very fine particles. It is typically washed and rounded or subangular in shape. Bunker sand, used in golf course bunkers, must satisfy requirements focused on player experience and drainage; USGA recommendations suggest a high percentage of particles between 0.25–1.0 mm, minimal fines, and appropriate angularity. Desert sand is a naturally occurring material with fine and rounded particles.

The first three sands (mason, golf, and bunker) were obtained from local suppliers in the State of Michigan, USA. The desert sand was obtained from a supplier in Saudi Arabia. The quartz (silica) sands were sourced from a national supplier in the USA and were used as reference materials owing to their common use in UHPC. Hereafter, the terms "quartz sand" and "silica sand" are used interchangeably. Fig. 1 shows the particle morphology of the sands, while Fig. 2 presents the particle size distributions of the fine aggregates.

All mixtures were reinforced with brass-coated, striated steel fibers, 13 mm in length and 0.20 mm in nominal diameter, with a minimum tensile strength of 2.93 GPa. Striated steel fibers were developed at the

Table 1
Mixture proportions by weight.

Materials	SS100	MS80	MS100	GS80	GS100	DS80	DS100	BS80	BS100
Cement	0.500	0.500	0.500	0.500	0.500	0.500	0.500	0.500	0.500
GGBS	0.500	0.500	0.500	0.500	0.500	0.500	0.500	0.500	0.500
Silica Fume	0.250	0.250	0.250	0.250	0.250	0.250	0.250	0.250	0.250
Water	0.219	0.219	0.219	0.219	0.219	0.219	0.219	0.219	0.219
Superplasticizer	0.035	0.035	0.035	0.035	0.035	0.035	0.035	0.035	0.035
Silica Sand F12	1.176	0.235		0.235		0.235		0.235	
Silica Sand F75	0.294	0.059		0.059		0.059		0.059	
Mason Sand		1.176	1.469						
Golf Sand				1.176	1.469				
Desert Sand						1.176	1.469		
Bunker Sand								1.176	1.469
Fiber (vol%)	1.5	1.5	1.5	1.5	1.5	1.5	1.5	1.5	1.5

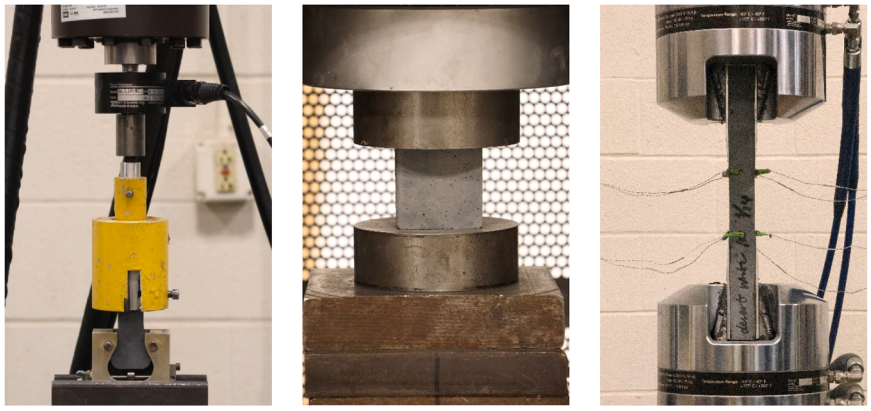

(a) (b) (c)

Fig. 4. Experimental setups for mechanical testing: (a) Single fiber pull-out test; (b) Compressive strength test; (c) Direct tensile test.

University of Michigan by El-Tawil [6] and have micron-scale surface markings designed to optimize their interactions with the UHPC matrix. For reference, brass-coated smooth steel fibers, also 13 mm in length and 0.20 mm in diameter, with a minimum tensile strength of 2.67 GPa, were used in the single-fiber pull-out test. The shapes of the steel fibers are shown in Fig. 3.

2.2. Mix design and specimen preparation

Nine series of UHPC mixtures were developed to examine the effects of sand type and blending ratio with silica sand on the mechanical performance of UHPC. The mix proportions are provided in Table 1. Specimen identifiers follow a consistent naming convention based on sand type and percentage. For example, “MS80” denotes a mix containing 80 % Mason sand and 20 % silica sand, while “DS100” refers to a mix made entirely with Desert sand. All mixtures incorporated striated steel fibers at a dosage of 1.5 % by volume, lower than the typical 2 % used in the U.S., and in line with the study’s general objective of reducing UHPC cost. This lower dosage was made feasible by the enhanced mechanical engagement offered by the striated fiber geometry, as discussed later.

A 40-liter laboratory planetary mixer was used to prepare the UHPC mixtures. First, silica fume was blended with all sand for approximately 5 min. Then, cement and GGBFS were added and mixed for an additional 5 min. Water and superplasticizer were gradually introduced into the dry mixture while the mixer was running. After the addition of water and superplasticizer, the mixture typically became fluid within 3 min. Once the mixture reached adequate consistency, steel fibers were incorporated and mixed until they were uniformly distributed. The fresh UHPC was cast into the molds from the center, allowing it to flow naturally into all four corners due to its high workability (spread of fresh UHPC $>$ 175 mm) and its self-compacting nature. After casting, the specimens were covered with plastic sheets and stored at room temperature for 24 h before demolding. The specimens were then transferred to a water bath maintained at 90 °C for 48 h to facilitate accelerated curing. All tests were conducted between 7 and 30 days after casting.

2.3. Tests conducted

A battery of tests was conducted to determine the fresh and hardened properties of the mixes. All mechanical property tests were conducted between 7 and 30 days after casting. These tests are:

- Flowability: The flowability of the UHPC mixes without steel fibers was evaluated using a flow test conducted in accordance with ASTM C230/C230M. No compaction or external vibration was applied to the flow table. Flow values were determined by averaging the diameters measured along two perpendicular directions.
- Single fiber pull-out test: Single fiber pull-out tests were conducted on 13 mm-long striated and smooth fibers using an MTS machine with a 100 kN capacity equipped with a 444 N (0.1kip) load cell. Each fiber was embedded 5 mm into the UHPC matrix and pulled out at a constant displacement rate of 0.0167 mm/s. A minimum of four specimens was tested for each mixture. The experimental setup is illustrated in Fig. 4(a).
- Compressive strength test: Compressive strength was measured following ASTM C109/C109M, using 50 $\times$ 50 $\times$ 50 mm cube specimens. The tests were performed on a Forney F-50F-F96 machine equipped with a 2.224 kN (500 kip) actuator. Loading was applied at the rate 0.25 MPa/s (36 psi/s). Fig. 4(b) shows the test setup. At least three specimens were tested per mixture.

Table 2
Compressive strength test results.

Series	SS100	MS80	MS100	GS80	GS100	DS80	DS100	BS80	BS100
Flowability (mm)	254	238	227	230	225	237	236	244	232
Strength (MPa)	191.6 (±4.36)	194.7 (±2.29)	183.8 (±4.40)	180.4 (±4.45)	178.6 (±5.19)	182.7 (±4.52)	178.4 (±6.71)	167.9 (±4.59)	176.5 (±4.51)

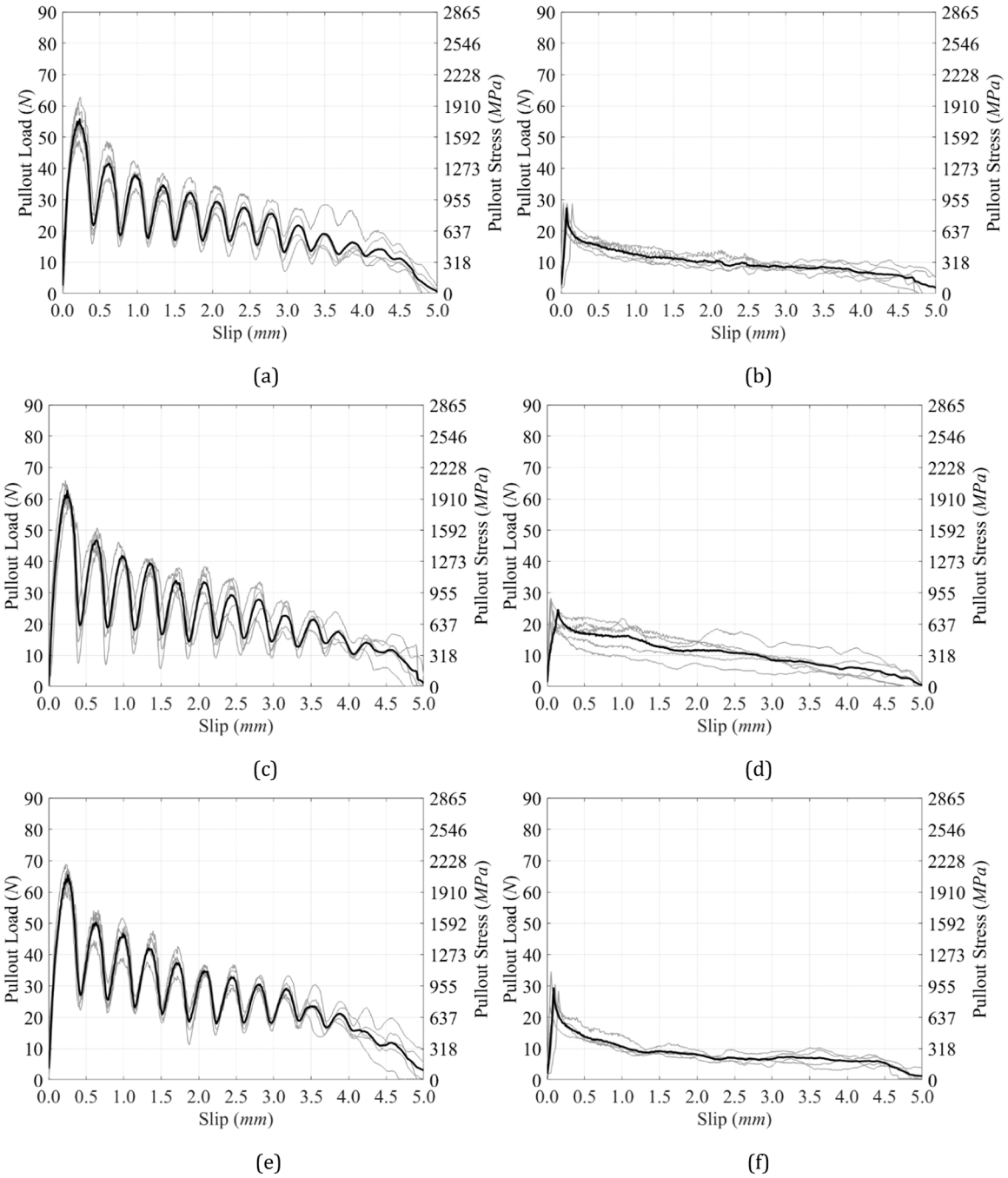

Fig. 5. Single-fiber pull-out load–slip responses of UHPC mixtures with various sands and two steel fiber types: (a) SS100–striated; (b) SS100–straight; (c) MS80–striated; (d) MS80–straight; (e) MS100–striated; (f) MS100–straight; (g) GS80–striated; (h) GS80–straight; (i) GS100–striated; (j) GS100–straight; (k) DS80–striated; (l) DS80–straight; (m) DS100–striated; (n) DS100–straight; (o) BS80–striated; (p) BS80–straight; (q) BS100–striated; (r) BS100–straight. (Note: * indicates fiber breakage observed in the BS80 and BS100 series).

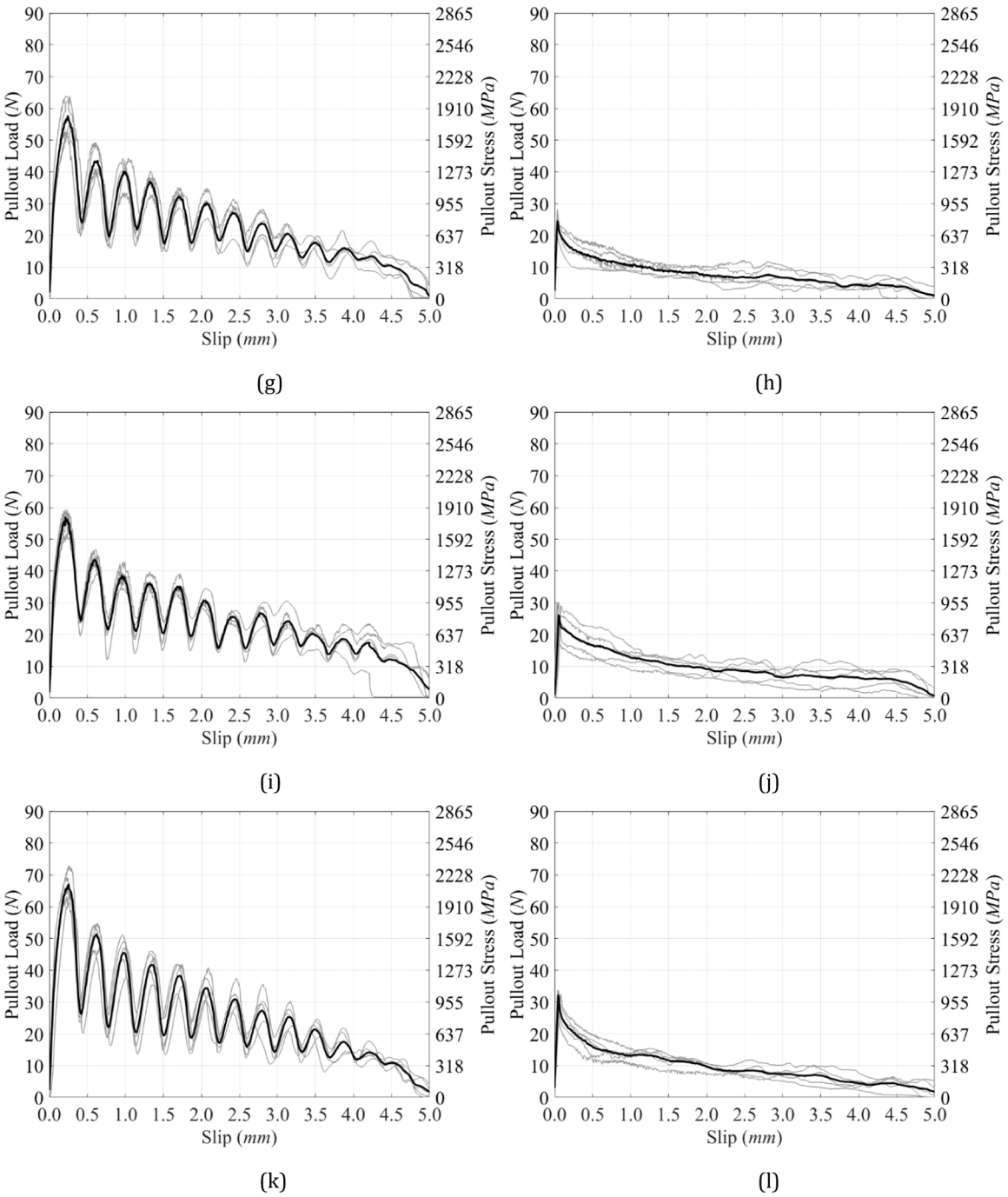

Fig. 5. (*continued*).

- Direct tensile test: Direct tension tests were conducted per the [1] standard. Coupons had a gage length of 95 mm and a 40 mm x 40 mm cross-section. Displacement-controlled loading was applied at the rate of 0.0025 mm/s using a servo-hydraulic MTS 810 system equipped with a 250 kN (55 kip) actuator. Five specimens were tested for each series, and the setup is shown in Fig. 4(c).

3. Experimental results

3.1. Flowability

Table 2 presents the flowability results for all UHPC mixtures. All mixtures satisfied the workability requirements typically expected of UHPC. Among them, the mixture prepared exclusively with silica sand exhibited the highest flowability, achieving a slump flow diameter of 257 mm, indicating superior rheological performance. In comparison, mixtures containing natural sands as full or partial replacements also showed adequate flowability, with average spread values around 233 mm. Notably, replacing 20 % of natural sand with silica sand slightly improved flowability compared to mixtures with only natural sand. This suggests that even limited substitution with silica sand can enhance the fresh-state performance of UHPC.

3.2. Compressive strength

The compressive strength results of UHPC mixtures incorporating

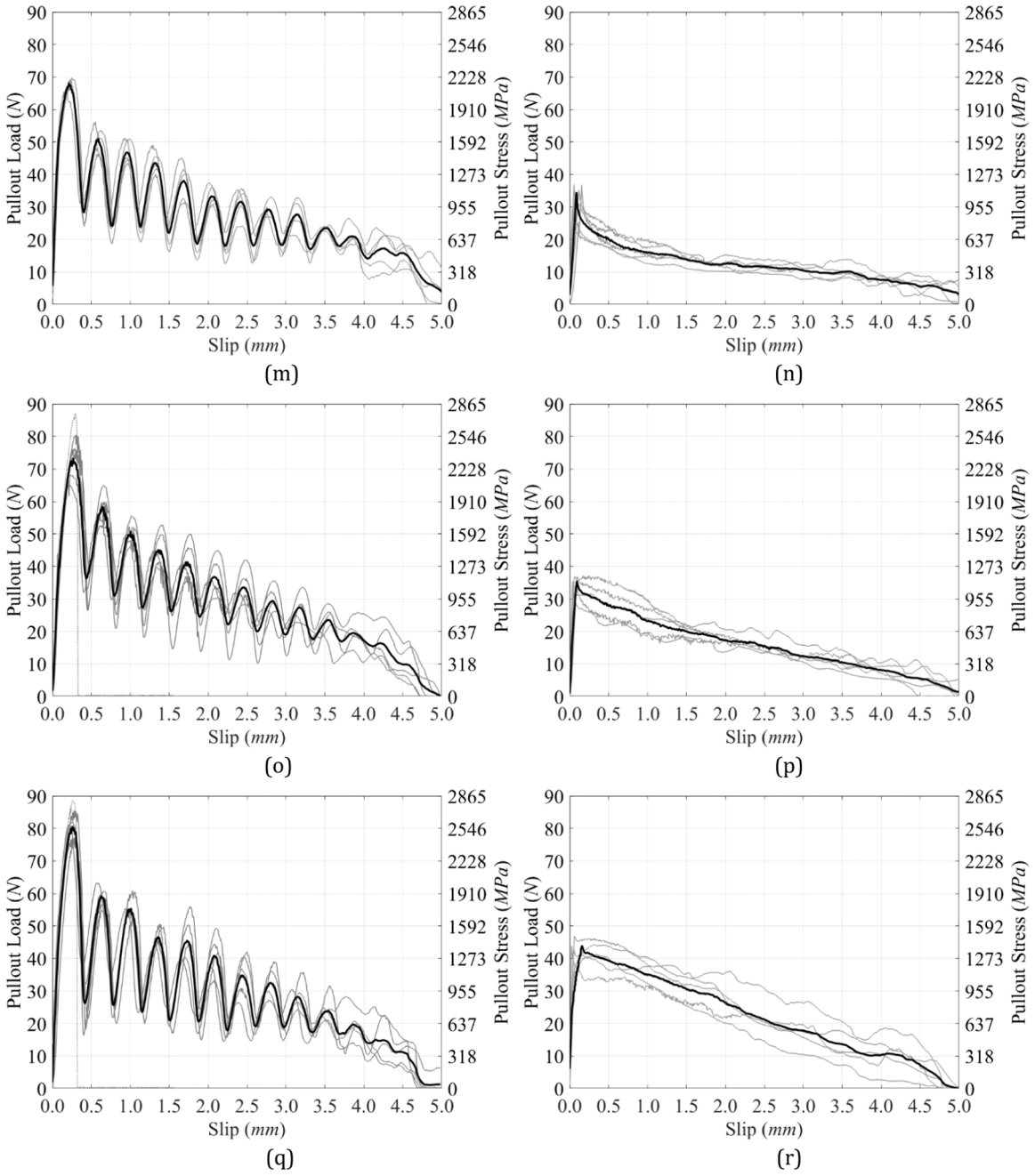

Fig. 5. (*continued*).

Table 3
Single-fiber pull-out test results of UHPC incorporating striated steel fiber.

Series	Max Pullout Load (N) (std)	Pullout Energy Density (MPa·mm) (std)	Equivalent Bond Strength (MPa)	Average Bond Strength (MPa)
SS100	55.81 (5.47)	3487 (467.5)	13.95	17.76
MS80	62.64 (2.47)	3692 (421.0)	14.77	19.94
MS100	65.47 (2.84)	4220 (267.3)	16.88	20.84
GS80	57.65 (5.86)	3552 (268.3)	14.21	18.35
GS100	56.89 (3.11)	3748 (394.2)	14.99	18.11
DS80	66.99 (4.06)	3938 (345.1)	15.75	21.32
DS100	68.00 (1.43)	4286 (314.1)	17.14	21.64
BS80	73.25 (6.32)	4531 (471.1)	18.13	23.32
BS100	80.61 (3.61)	4557 (231.4)	18.23	25.66

Table 4
Single-fiber pull-out test results of UHPC incorporating smooth steel fiber.

Series	Max Pullout Load (N) (std)	Pullout Energy Density (MPa·mm) (std)	Equivalent Bond Strength (MPa)	Average Bond Strength (MPa)
SS100	27.33 (2.39)	1554 (250.5)	6.18	8.70
MS80	24.54 (3.62)	1676 (454.3)	6.70	7.81
MS100	29.33 (4.55)	1315 (233.5)	5.26	9.34
GS80	24.53 (2.90)	1232 (310.0)	4.93	7.81
GS100	26.12 (5.34)	1510 (465.4)	6.04	8.32
DS80	32.20 (2.05)	1507 (202.5)	6.03	10.25
DS100	34.41 (3.12)	1923 (227.5)	7.69	10.95
BS80	35.33 (1.85)	2500 (246.7)	10.00	11.25
BS100	43.86 (2.06)	3519 (629.9)	14.08	13.96

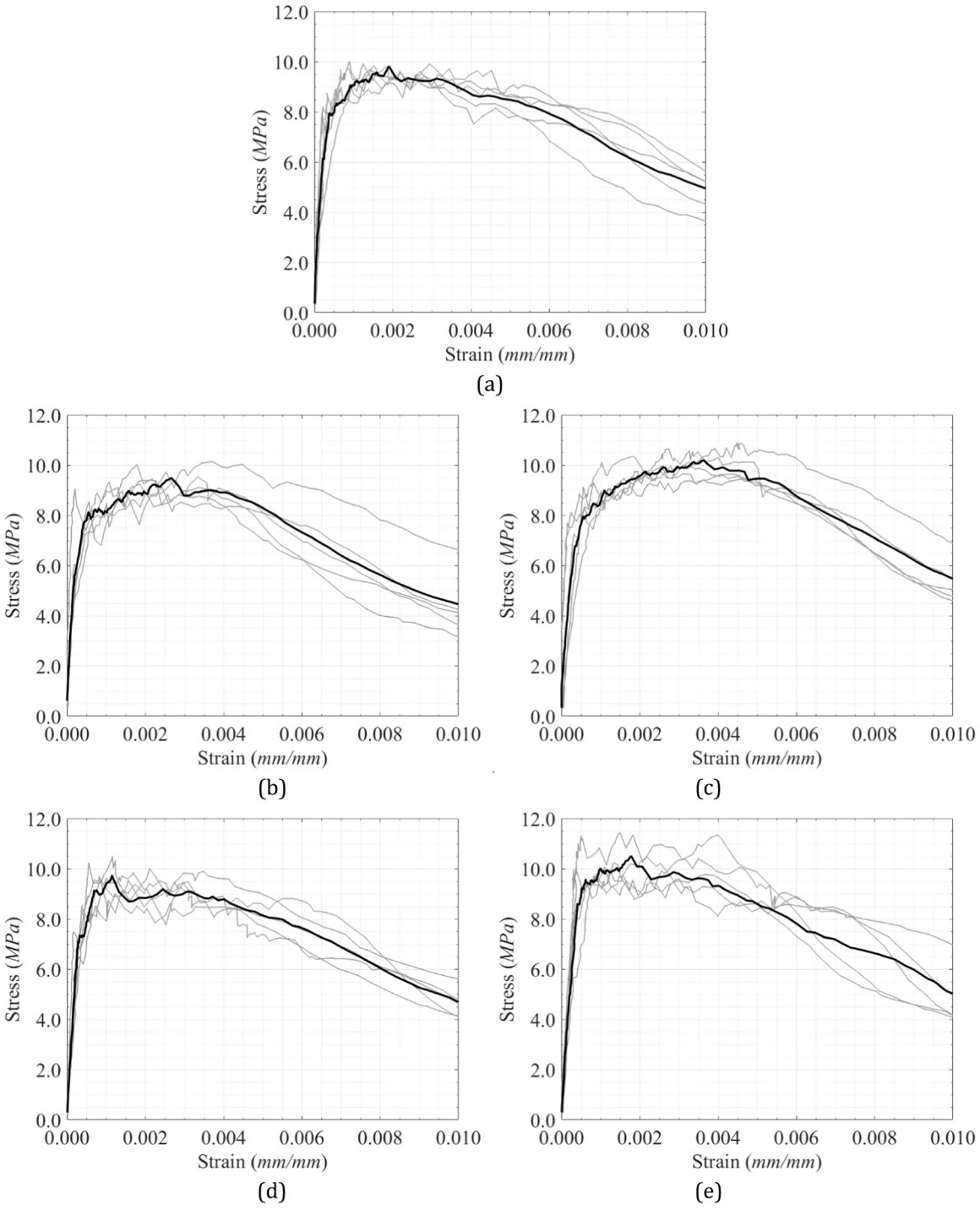

Fig. 6. Tensile stress and strain curves of UHPC: (a) SS100; (b) MS80; (c) MS100; (d) GS80; (e) GS100; (f) DS80; (g) DS100; (h) BS80; (i) BS100.

different sand types are presented in Table 2. All mixtures well exceeded 150 MPa, reaffirming their qualification as UHPC. The reference mixture containing 100 % silica sand (SS100) achieved 191.6 MPa and served as the baseline for comparison. Notably, the mixture with 80 % Mason sand (MS80) attained the highest strength at 194.7 MPa, slightly surpassing the reference. This indicates that certain natural sands, when optimally blended with silica sand, can match or even outperform conventional UHPC in terms of compressive strength. A similar trend was observed for Golf sand and Desert sand, where partial replacements (GS80 and DS80) yielded higher strengths than their full-replacement counterparts (GS100 and DS100). In contrast, the Bunker sand series produced the lowest strengths among all tested mixtures, ranging from 167.9 MPa (BS80) to 176.5 MPa (BS100), yet still within acceptable UHPC performance thresholds (>150 MPa).

These results demonstrate that natural sands can replace silica sand in UHPC without significantly compromising compressive strength, particularly when used in partial substitution. The observed strength variations suggest that factors beyond particle packing density, such as sand angularity and surface texture, may significantly affect the compressive response of UHPC. The interaction between the sand and

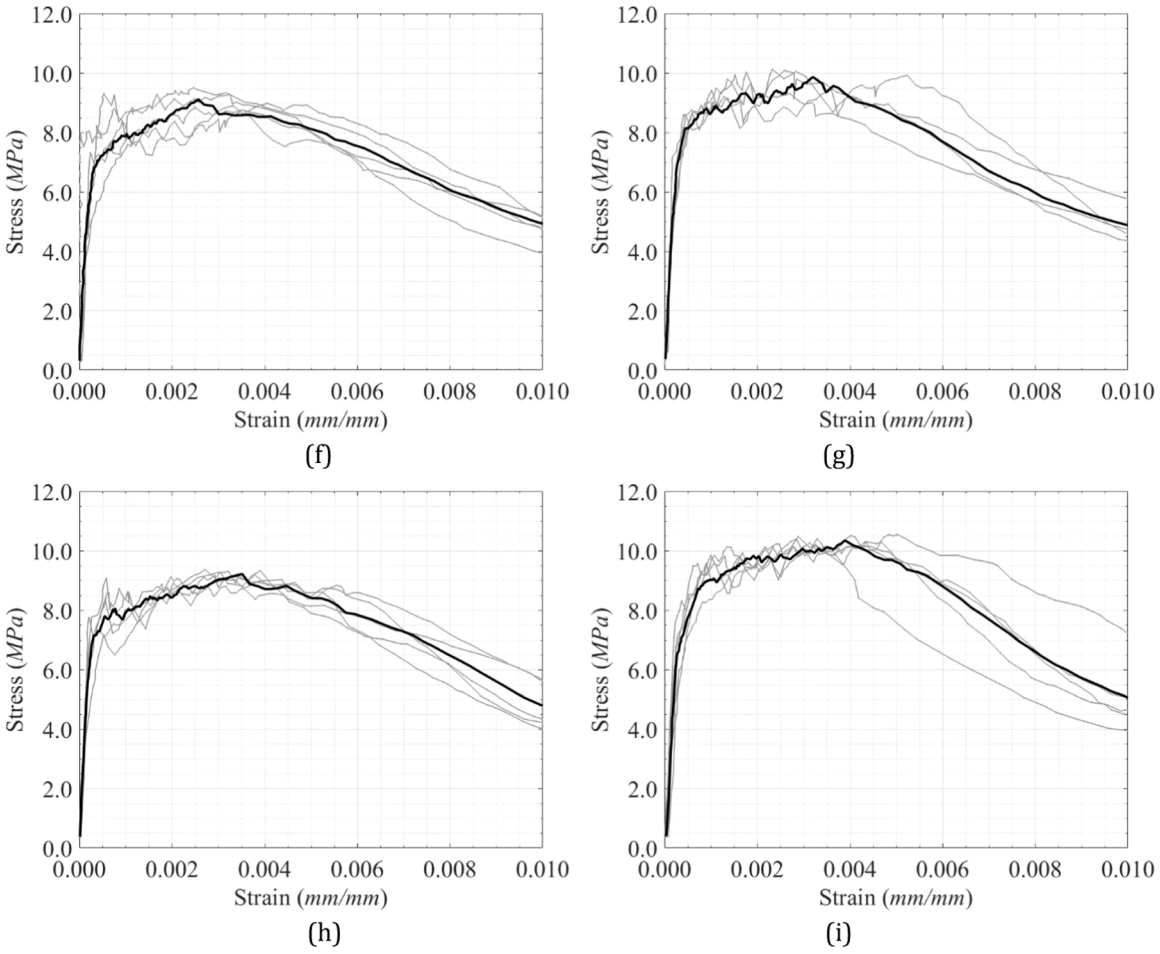

Fig. 6. (*continued*).

Table 5
Summary of tensile stress–strain properties of UHPC incorporating striated steel fiber.

Series	Cracking Strain (mm/mm)	First Cracking Stress (MPa)	Strain at Max Stress (mm/mm)	Max Stress (MPa)	Localization Strain (mm/mm)	Localization Strength (MPa)
SS100	0.00038 (±0.00004)	7.95 (±0.49)	0.0019 (±0.0007)	9.80 (±0.25)	0.0031 (±0.0003)	9.32 (±0.28)
MS80	0.00042 (±0.00007)	7.65 (±0.44)	0.0027 (±0.0006)	9.48 (±0.45)	0.0039 (±0.0002)	8.92 (±0.70)
MS100	0.00038 (±0.00005)	6.77 (±1.11)	0.0036 (±0.0008)	10.19 (±0.47)	0.0041 (±0.0002)	9.91 (±0.53)
GS80	0.00032 (±0.00014)	7.32 (±1.44)	0.0012 (±0.0002)	9.72 (±0.55)	0.0032 (±0.0002)	9.09 (±0.56)
GS100	0.00040 (±0.00003)	8.60 (±1.10)	0.0018 (±0.0006)	10.50 (±0.65)	0.0037 (±0.0003)	9.54 (±0.19)
DS80	0.00032 (±0.00013)	6.76 (±0.30)	0.0026 (±0.0003)	9.11 (±0.20)	0.0041 (±0.0004)	8.55 (±0.47)
DS100	0.00043 (±0.00009)	8.08 (±0.03)	0.0032 (±0.0004)	9.86 (±0.40)	0.0045 (±0.0003)	8.89 (±0.34)
BS80	0.00030 (±0.00005)	7.12 (±0.44)	0.0035 (±0.0003)	9.21 (±0.24)	0.0052 (±0.0001)	8.39 (±0.45)
BS100	0.00030 (±0.00004)	6.21 (±0.54)	0.0039 (±0.0003)	10.35 (±0.18)	0.0055 (±0.0004)	9.28 (±0.74)

the cementitious matrix, influenced by these morphological characteristics, likely plays a key role in stress transfer and densification during curing. Thus, both material selection and mix proportioning strategies are critical when designing UHPC with alternative fine aggregates.

3.3. Single fiber pull-out test

To evaluate the fiber–matrix interfacial properties in UHPC incorporating various natural sands, single-fiber pull-out tests were conducted using both striated and smooth steel fibers. Fig. 5 presents the pull-out load–slip responses of each mixture, showing both the raw data and the averaged curves. The averaging method follows an earlier work

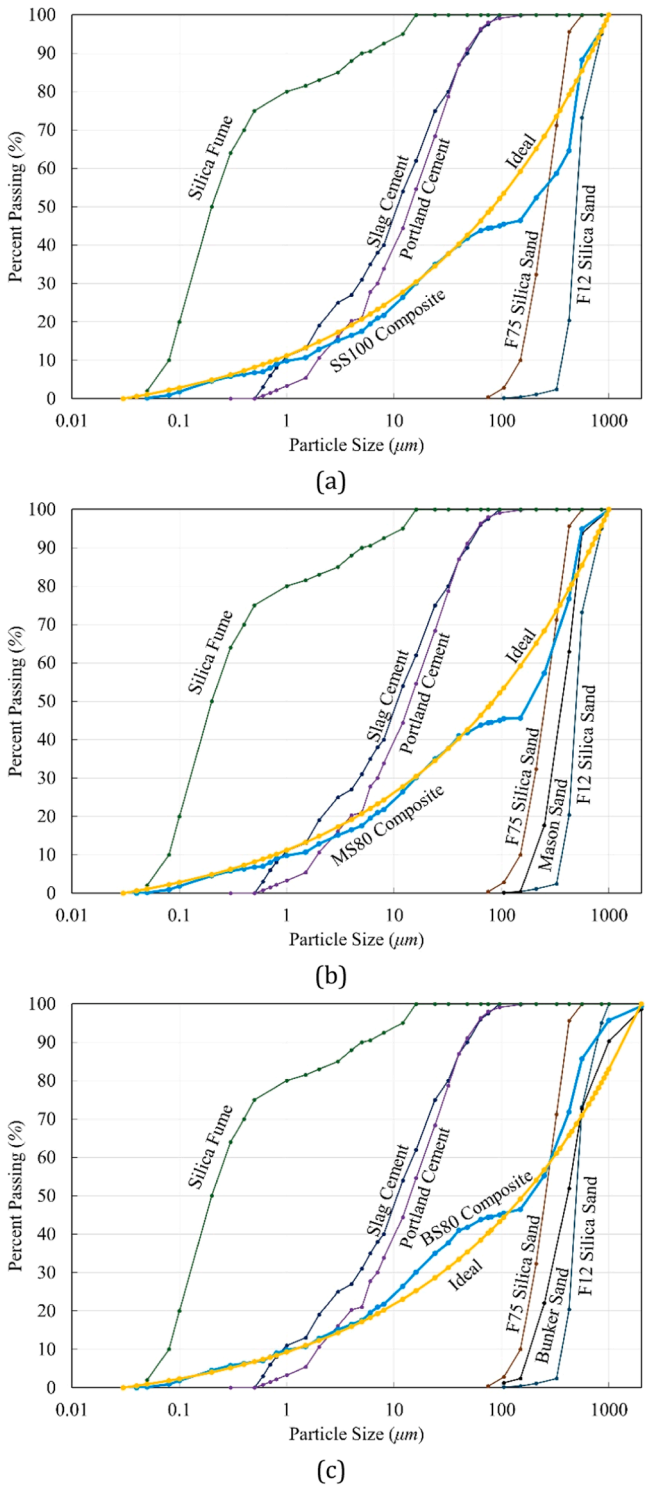

Fig. 7. Particle size distribution of solid constituents and comparison between measured and predicted packing curves based on the Modified Andreasen particle packing model: (a) SS100 series; (b) MS80 series; (c) BS80 series.

by the authors [19]. Tables 3 and 4 summarize the corresponding mechanical metrics, including maximum pull-out load, pull-out energy density, equivalent bond strength, and average bond strength. Unlike the well-known generally descending post-peak response of smooth fibers, the striated fibers exhibit a unique oscillating response as shown in Fig. 5. This is due to the periodic interactions that occur between the striations and the surrounding matrix as the pullout process progresses.

The pull-out energy density was calculated as the area under the pull-out stress versus slip curve, where the pull-out stress is computed from the tensile force transmitted through the fiber during extraction, i.e., pull-out force divided by fiber cross-sectional area. The pull-out energy density is computed up to the point of complete fiber removal and then used to compute the equivalent bond strength (τ_{eq}). The equivalent bond strength was proposed by Kim et al. [14] and Wille and Naaman [24] and is expressed in Eq. (1):

$$\tau_{eq} = \frac{pullout\ energy\ density \times d_f}{2 \bullet L_E^2} \tag{1}$$

where d_f is the fiber diameter and L_E is the initial embedment length. It reflects a uniform interfacial bond stress along the embedment length and measures the energy dissipation efficiency of the pull-out process.

Additionally, the average bond strength (τ_{av}) was calculated based on the maximum pull-out load $P_{\max}$, following Wille and Naaman [24] and as shown in Eq. (2):

$$\tau_{av} = \frac{P_{\max}}{\pi \times d_f \times L_E} \tag{2}$$

This value is a measure of the bond stress under the assumption of a uniformly distributed interfacial load.

The results consistently show that striated fibers outperform smooth fibers in all UHPC mixtures. For example, the reference mixture (SS100) with striated fibers reached a maximum pull-out load of 55.8 N and a pull-out energy density of 3487 MPa·mm, which are more than double the corresponding quantities for the smooth fiber, i.e. 27.3 N and 1554 MPa·mm, respectively. The average bond strength is also nearly double (17.76 MPa compared to 8.70 MPa).

Among the natural sand blends, bunker sand (BS100) exhibited the highest pull-out performance. Notably, instances of fiber breakage were observed in both BS80 and BS100 series, as shown in Fig. 5. To ensure fair comparison of pull-out energy density, these breakage cases were excluded from the test results summarized in Table 3. With striated fibers, BS100 achieved the maximum pull-out load (80.6 N), the greatest pull-out energy density (4557 MPa·mm), and the highest equivalent bond strength (18.23 MPa). The average bond strength in this case reached 25.66 MPa. Even with smooth fibers, BS100 demonstrated superior performance, suggesting that the particle size distribution, surface morphology, and angularity of bunker sand may significantly enhance fiber–matrix bonding. Desert sand (DS100) showed excellent performance, achieving a maximum load of 68.0 N and energy density of 4286 MPa·mm with striated fibers, which corresponds to a high equivalent bond strength of 17.14 MPa. This performance was comparable to or exceeded that of silica sand–based mixtures, demonstrating the viability of using widely available natural sands in UHPC.

Mixtures with mason sand (MS) and golf sand (GS) exhibited bond performance that was comparable with the reference SS mixture. For example, MS100 with striated fibers delivered a maximum load of 65.5 N and equivalent bond strength of 16.88 MPa, while GS100 showed a load of 56.9 N and a bond strength of 14.99 MPa. These trends were mirrored in the smooth fiber tests.

Overall, the results confirm that both fiber geometry and aggregate type critically influence pull-out behavior. The strong performance of UHPC mixtures with bunker and desert sands suggests that factors beyond particle packing density, such as grain shape, angularity, and particle size distribution, may significantly enhance the mechanical bond between the fiber and the matrix. These are explored later.

3.4. Direct tension tests

Fig. 6 displays the tensile stress–strain responses of UHPC mixtures incorporating the various types of sand, with individual curves and one averaged curve shown per mixture. Table 5 summarizes key tensile parameters, including cracking strain and stress, strain and stress at peak load, and localization strain, calculated following the methodology

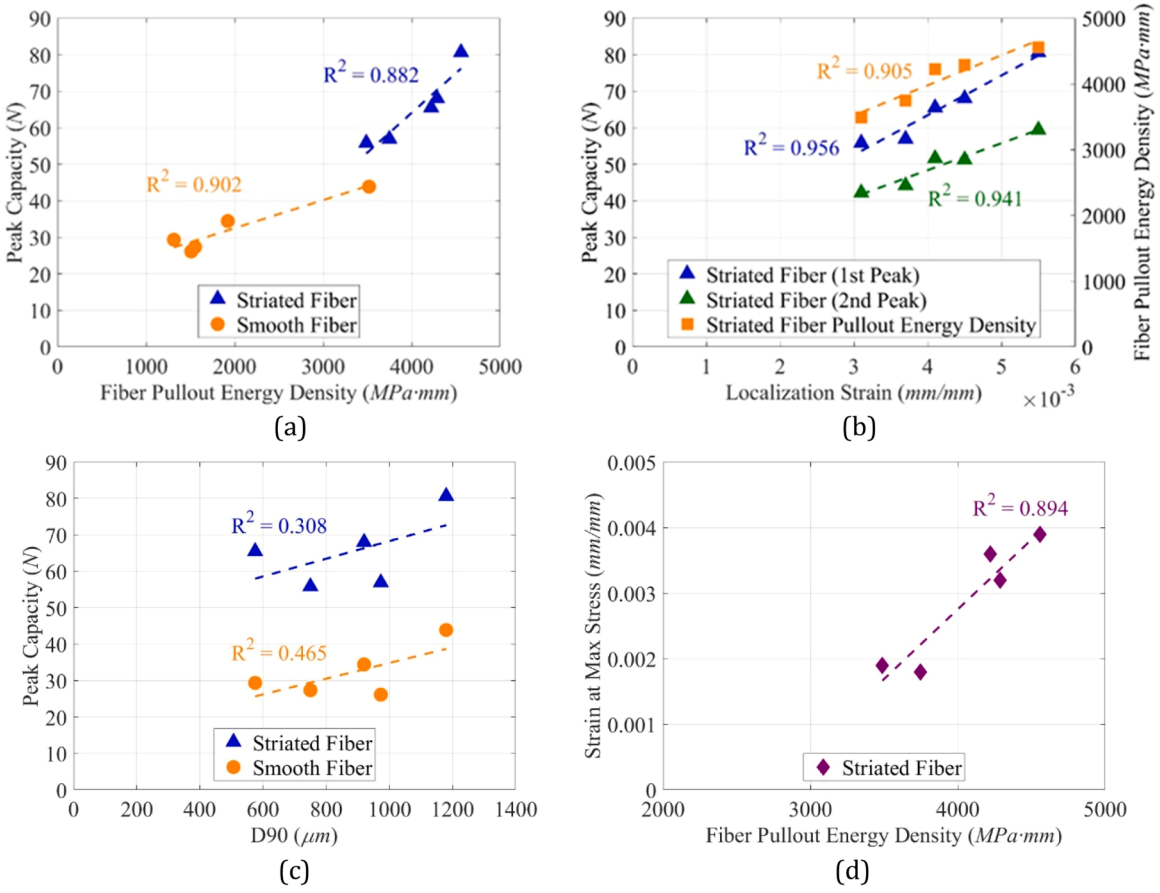

Fig. 8. (a) Relationship between peak capacity of single fiber pull-out test and peak capacity of single fiber pull-out test; (b) Relationship between peak capacity and fiber pull-out energy density of single fiber pull-out test and localization strain of UHPC; (c) Relationship between D90 particle size sand and peak capacity of single fiber pull-out test; (d)Relationship between pullout energy density of single striated fiber and the strain at max stress in the tensile test.

proposed by Saqif and El-Tawil [20].

All mixtures exhibited characteristic strain-hardening behavior after initial cracking, indicative of effective fiber bridging provided by the embedded striated steel fibers. The reference mixture (SS100) achieved a cracking stress of 7.95 MPa and a maximum tensile stress of 9.80 MPa at a strain of 0.0019. The corresponding localization strain was 0.0031, with a localization tensile strength of 9.32 MPa.

Among the mixtures using natural sands, BS100 demonstrated high tensile capacity, with a maximum stress of 10.35 MPa, and the highest localization strain (0.0055). MS100 and GS100 showed competitive tensile strengths of 10.19 MPa and 10.50 MPa, respectively, with good ductility. DS100 also performed well, reaching 9.86 MPa at a strain of 0.0032 and maintaining post-peak deformation up to 0.0045.

The tensile trends do not fully mirror those observed in the compressive tests. For example, GS80 had higher compressive strength than GS100, yet the opposite was observed in tensile capacity. This reflects fundamental differences in governing mechanisms: compressive strength in UHPC is largely influenced by dense particle packing, whereas tensile behavior depends more on matrix properties and fiber–matrix bonding. In particular, cracking strain is generally governed by the matrix, while post-cracking resistance is strongly affected by the quality of fiber bridging. This observation is further supported by the single-fiber pull-out test results. For example, the BS100 mixture had among the lowest compressive strengths of all the mixtures. However, it had the greatest fiber pull-out load (80.6 N), energy density (4557 MPa·mm), and average bond strength (25.66 MPa) among all the mixtures. The strong interfacial bond in BS100 likely contributed to the superior tensile performance of its mix by enabling effective bridging through delayed fiber debonding and pull-out. DS100 also exhibited high pull-out performance, consistent with its enhanced tensile behavior.

Overall, these findings demonstrate that UHPC mixtures incorporating well-selected natural sands, particularly bunker and desert sands, can match or exceed the tensile performance of silica sand–based UHPC. The results highlight the critical role of fiber–matrix bonding in governing tensile resistance and point to the potential of natural sand alternatives for use in high-performance applications.

4. Discussion of experimental results

The particle packing efficiency of UHPC mixtures was assessed using the Modified Andreasen Model [4], with a power $q = 0.25$, see Eq. 3. A commonly used value for optimal packing of powders is $q = 0.37$. However, for mixtures with a high amount of fine powders (<250 μm), a smaller q value is recommended by Brouwers and Radix [3] and [11]. Hunger [10] suggested q values in the range of 0.22~0.25 for self-consolidating concrete, hence the selection made in this work.

$$CPFT(d) = 100 \quad \left(\frac{d^q - d_{\min}^q}{d_{\max}^q - d_{\min}^q}\right) \tag{3}$$

where CPFT(d) denotes the cumulative percent finer than particle size d, and $d_{\min}$ and $d_{\max}$ represent the minimum and maximum particle sizes, respectively.

As illustrated in Fig. 7, both SS100 and MS80 closely followed the ideal particle size distribution curve and achieved similar levels of compressive strength, approximately 193–195 MPa. In contrast, the BS80 mixture showed a modest deviation from the ideal curve, which is

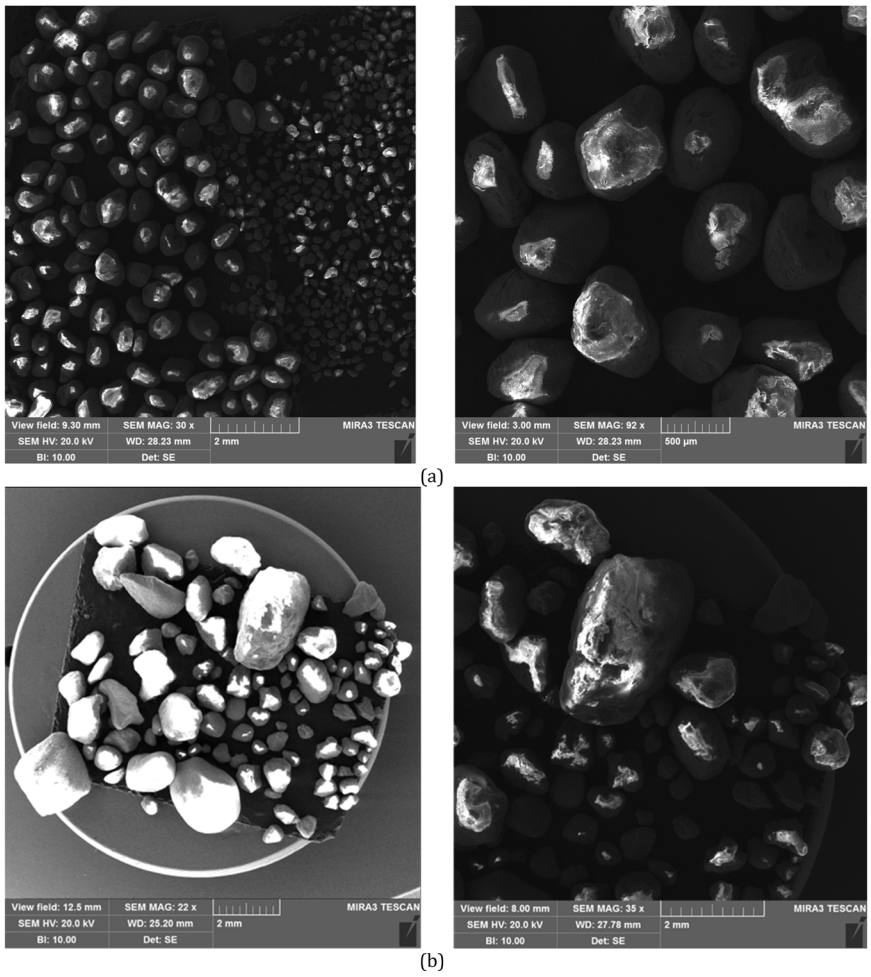

Fig. 9. SEM images of particle shape of (a) silica sand and (b) Bunker sand.

likely the reason for its comparatively lower compressive strength (169.3 MPa). These observations are in line with established UHPC design principles, where improved particle packing reduces porosity, enhances matrix homogeneity, and results in higher compressive strength.

While compressive strength is governed primarily by packing density, tensile performance is more closely related to fiber–matrix interaction. As shown in Fig. 8(a), pull-out energy density and peak pull-out load demonstrated a strong linear correlation across both striated and smooth fibers. Mixtures with striated fibers exhibited significantly higher energy absorption and peak load values, confirming the effectiveness of mechanical interlock in improving interfacial resistance. These trends extended to composite-scale behavior. Fig. 8(b) indicates that UHPC mixtures with higher pull-out energy and peak load also developed greater tensile strength and localization strain, further highlighting the importance of fiber bridging in resisting crack propagation.

An important observation emerged from Fig. 8(c), which shows a positive trend between the D90 particle size of sand and the peak pull-out capacity. Although D90 alone does not fully characterize sand behavior, larger average particle sizes appear to improve the mechanical interaction at the fiber–matrix interface in the mixtures studied. This finding suggests that particle size influences the local stress transfer environment around fibers, potentially by altering micro-confinement, general frictional conditions, and/or through physical interaction with the striations during pull-out. Furthermore, the relationship between fiber pull-out energy density and composite tensile strain capacity was examined, as shown in Fig. 8(d). A strong correlation ($R^2 = 0.894$) indicates that mixtures with higher pull-out energy density developed greater strain at maximum stress. This explains the behavior of the GS mixture, which achieved the highest tensile strength from strong fiber–matrix bonding but showed the lowest strain capacity. Its limited pull-out energy restricted strain development, emphasizing that UHPC ductility depends not only on interfacial bond strength but also on sufficient energy absorption to sustain multiple cracking and strain localization.

Scanning electron microscopy (SEM) images presented in Fig. 9 compare the surface morphology of the two types of silica sand (F12 and F75) and Bunker sand. Particles of both types of silica sands appear smooth and rounded, whereas Bunker sand particles are more angular and rough-textured. The SEM images of the particles were post-processed using ImageJ software [21] to compute the geometric characteristics of the sand particles. The images were first adjusted to increase intensity contrast and then binarized to enable further region extraction using Matlab's *bwboundaries* function [17]. A measure of Angularity (Eq. (4)), adopted from Su and Yan [22] and originally proposed by Masad et al. [16], along with Circularity (Eq. (5)), obtained using Matlab' *regionprops* function [17], were computed for each extracted region.

$$Angularity = \sum_{i=0}^{\frac{2\pi}{\Delta\varphi}-1} \frac{\left| r_{p(i\Delta\varphi)} - r_{EE(i\Delta\varphi)} \right|}{r_{EE(i\Delta\varphi)}} \tag{4}$$

where $\Delta\varphi = 5^\circ$ is the angular step size used in the summation, $r_{p(i\Delta\varphi)}$ is the radius of the particle and $r_{EE(i\Delta\varphi)}$ is the radius of an equivalent ellipse

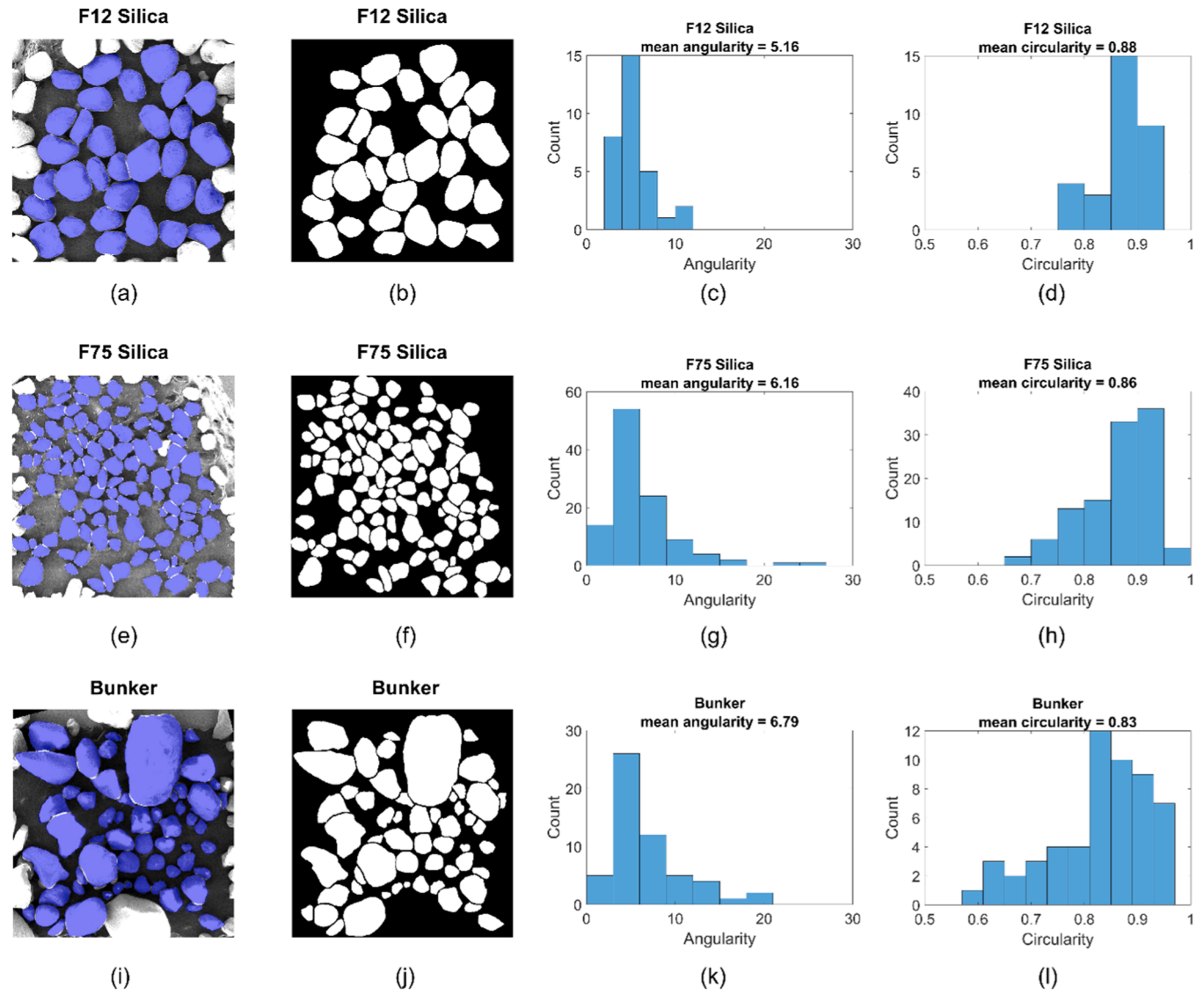

Fig. 10. Shape analysis results for F12 silica, F75 silica, and bunker sand. (a), (e), (i): Extracted particles (shown in blue) overlaid on high-contrast images. (b), (f), (j): Binary plots of the analyzed particles. (c), (g), (k): Histograms of angularity. (d), (h), (l): Histograms of circularity.

Table 6
Mean angularity and circularity of sand particles.

Sand type	Mean angularity	Mean Circularity
F12 Silica sand	5.16	0.88
F75 Silica sand	6.16	0.86
Silica sand mix	5.36	0.88
Bunker sand	6.79	0.83

at the directional angle $i\Delta\varphi$.

$$Circularity = \frac{4\pi \bullet Area}{Perimeter^2} \times \left(1 - \frac{0.5}{r}\right)^2 \quad (5a)$$

where r is given by:

$$r = \frac{Perimeter}{2\pi} + 0.5 \quad (5b)$$

Fig. 10 (a), (e), and (i) show extracted particle outlines overlaid on high-contrast images of three sand types. To ensure accurate shape analysis, particles at image edges, those heavily occluded by others, or those poorly separated from the background due to lighting effects were excluded. The corresponding binary images (Fig. 10 (b), (f), and (j)) display the particles included in the analysis, while angularity and circularity indices for individual particles are summarized in the histograms (Fig. 10 (c)–(d), (g)–(h), and (k)–(l)). Table 6 presents the mean values of angularity and circularity indices for each sand type, as well as for the "silica sand mix," which represents the weighted mean values for F12 and F75 silica sands combined in a 4:1 ratio, as outlined in Table 1. The silica sand mix exhibits a 21 % lower mean angularity and a 6 % higher mean circularity compared to bunker sand. Generally, sands with higher angularity and lower circularity provide greater resistance to fiber pull-out because their shape increases the likelihood of physically impeding fiber extraction, for example, through surface abrasion (scratching) for both smooth and striated fibers or through mechanical interlocking at the edges of the striations for the latter.

It should be noted that the morphological data for each sand type were obtained by randomly selecting particles from a single SEM image. While this approach minimizes selection bias, it may not fully capture the broader morphological variability present in the bulk sample, an important limitation to consider when interpreting these results. Nonetheless, the observed morphological distinctions directly influenced interfacial bonding behavior and help explain the significantly higher fiber pull-out strength observed in specimens containing bunker

sand compared to those with silica sand.

The BS100 mixture, which incorporated Bunker sand, achieved the highest pull-out load (80.6 N), average bond strength (25.66 MPa), and pull-out energy density (4557 MPa·mm), despite exhibiting lower packing efficiency than SS100 or MS80. This enhancement was attributed to increased friction and mechanical interlock between fibers and the surrounding matrix. The superior performance of desert sand mixtures (e.g., DS100) further supports this interpretation. Notably, even with smooth fibers, the BS100 mixture still demonstrated favorable pull-out results, emphasizing the role of aggregate morphology in enhancing bond strength.

These findings indicate that conventional metrics such as D90 and packing density are insufficient to fully describe the fiber–matrix interaction. While D90 showed some correlation with pull-out performance in this study, it is the combination of particle size, shape, angularity, and surface roughness that governs the bond behavior. Therefore, aggregate selection for UHPC should account for these morphological parameters in addition to gradation.

5. Conclusion

This study clearly established that regionally sourced natural sands, such as mason, golf, desert, and bunker sands, are viable substitutes for high-purity quartz sand in ultra-high performance concrete (UHPC). These sand types are up to 95 % cheaper than quartz sand and can be utilized to fully or partially replace quartz sand without compromising the essential engineering properties of UHPC. The key observations and findings of this study can be summarized as follows:

1. Mason, golf, desert, and bunker sands can fully or partially replace high-purity quartz sand in UHPC while maintaining compressive strength above 150 MPa. Several partial-replacement mixes matched or exceeded the reference silica sand mixture. In terms of workability, the reference silica sand mixture exhibited the highest flowability with a slump flow of 257 mm, while natural sand mixtures achieved satisfactory values, near 233 mm.
2. Aggregate morphology, particularly particle angularity and surface roughness, strongly influences UHPC's mechanical and interfacial performance. Mixtures with bunker and desert sands, characterized by highly angular and textured particles, exhibited the greatest fiber–matrix bond strength and pull-out energy. This resulted in superior tensile strength, pronounced strain hardening, and enhanced post-cracking ductility, highlighting the central role of fiber–matrix interaction in achieving composite toughness. By contrast, the golf sand mixture, although attaining the highest tensile strength due to strong fiber–matrix bonding, showed the lowest strain capacity because of its relatively low fiber pull-out energy density. This outcome emphasizes that UHPC ductility depends not only on interfacial bond strength but also on sufficient energy absorption to sustain multiple cracking and strain localization.
3. SEM and quantitative image analysis confirmed that angular, rough-surfaced particles promote mechanical interlock and energy dissipation, indicating that both particle gradation and morphological characteristics are necessary to predict fiber–matrix performance.
4. The newly introduced striated fibers significantly improved interfacial bonding compared with smooth fibers, amplifying the positive effects of sand morphology on composite tensile performance.

This research confirms that well-selected and well-proportioned local natural sands can reliably substitute for quartz sand in UHPC, maintaining or improving workability, compressive strength, and tensile ductility while substantially reducing cost and environmental impact. These findings provide a technical basis for expanding aggregate selection criteria to include morphological characteristics and support the development of economical, high-performance, and sustainable UHPC for widespread structural applications. Nonetheless, this study was limited in mechanistic scope, as it did not include analyses of pore structure or hydration degree. Future research should address these aspects, along with microstructural characterization and the pull-out mechanism of striated fibers through advanced numerical or analytical approaches.

CRediT authorship contribution statement

Zhengye Tang: Writing – original draft, Visualization, Investigation, Formal analysis, Data curation. **Min-Chun Han:** Writing – review & editing, Visualization, Software, Investigation, Formal analysis, Data curation. **Sherif El-Tawil:** Writing – review & editing, Supervision, Resources, Project administration, Methodology, Funding acquisition, Conceptualization. **Sukhoon Pyo:** Writing – review & editing, Investigation, Formal analysis.

Declaration of Competing Interest

The authors declare the following financial interests/personal relationships which may be considered as potential competing interests: The striated steel fibers used in this study were manufactured by HiPer Fiber, Inc. and provided to the University of Michigan for use in this research. The senior author, Sherif El-Tawil, holds a significant ownership interest in HiPer Fiber, Inc. The underlying patent for the fiber design is owned by the University of Michigan and is exclusively licensed to HiPer Fiber, Inc. The conflict of interest arising from these relationships is managed by the Conflict of Interest Office at the University of Michigan.

Acknowledgement

This research was supported jointly by the University of Michigan and the Michigan Department of Transportation (MDOT). Any opinions, findings, conclusions, and recommendations expressed in this paper are those of the authors and do not necessarily reflect the views of the sponsors. The last author was supported by the National Research Foundation of Korea (NRF) grant funded by the Korea government (MSIT) (No. RS-2023–00212366 and RS-2024–00399324). The authors also wish to thank Mr. Naif Aljohani for procuring the desert sand used in this study and for his assistance with experimental testing.

Data availability

Data will be made available on request.

References

[1] AASHTO, AASHTO T397-22: standard method of test for uniaxial tensile response of ultra-high performance concrete, American Association of State Highway and Transportation Officials, Washington, DC, 2022.
[2] M. Alkaysi, S. El-Tawil, Effects of variations in the mix constituents of ultra high performance concrete (UHPC) on cost and performance, Mater. Struct. 49 (2016) 4185–4200.
[3] H.J.H. Brouwers, H.J. Radix, Self-compacting concrete: theoretical and experimental study, Cem. Concr. Res. 35 (11) (2005) 2116–2136.
[4] H.J.H. Brouwers, H.J. Radix, Self-compacting concrete: the role of the particle size distribution, first Int. Symp Des. Perform. Use SCC Hunan China (2005) 109–118.
[5] D. Choi, K. Hong, M. Ochirbud, D. Meiramov, P. Sukontaskuul, Mechanical properties of ultra-high performance concrete (UHPC) and ultra-high performance fiber-reinforced concrete (UHPFRC) with recycled sand, Int. J. Concr. Struct. Mater. 17 (1) (2023) 67.
[6] S. El-Tawil, High bond steel fibers for ultra high-performance concrete (UHPC). NCHRP IDEA project 235, transportation research board, Natl. Acad. Sci. Eng. Med. Wash. DC (2022). ⟨https://onlinepubs.trb.org/onlinepubs/IDEA/FinalReports/Highway/NCHRP235.pdf⟩.
[7] S. El-Tawil, M. Saqif, W. Hazelton, J. Winckler, M. Clark, "Construction of a Short-Span UHPC bridge: cost considerations and lessons learned, Concr. Int. 47 (2) (2025).
[8] S. El-Tawil, Y.S. Tai, J.A. Belcher II, D. Rogers, Open-recipe ultra-high-performance concrete, Concr. Int. 42 (6) (2020) 33–38.

[9] C.C. Hung, S. El-Tawil, S.H. Chao, A review of developments and challenges for UHPC in structural engineering: behavior, analysis, and design, J. Struct. Eng. 147 (9) (2021) 03121001.
[10] M. Hunger, *an integral design concept for ecological self-compacting concrete* (Ph.D. dissertation), Eindh. Univ. Technol. Eindh. Neth. (2010).
[11] G. Hüsken, H.J.H. Brouwers, A new mix design concept for earth-moist concrete: a theoretical and experimental study, Cem. Concr. Res. 38 (10) (2008) 1246–1259.
[12] M.C. Kang, M. Kang, G. Jun, Y. Oinam, H.M. Seung, S. Pyo, Electrical and mechanical characteristics of CaO-activated cementless ultra-high performance concrete (UHPC) incorporating steel slag aggregates, Dev. Built Environ. 23 (2025) 100713.
[13] M.C. Kang, B. Lee, M. Kang, S.J. Lee, S. Pyo, Self-sensing properties of cementless ultra-high performance concrete (UHPC) with slag aggregates, J. Build. Eng. 86 (2024) 108863.
[14] D.J. Kim, S. El-Tawil, A.E. Naaman, Loading rate effect on pullout behavior of deformed steel fibers, Acids Mater. J. 105 (6) (2008) 576.
[15] F. Li, T. Yao, J. Luo, Q. Song, T. Yang, R. Zhang, M. Li, Experimental investigation on the performance of ultra-high performance concrete (UHPC) prepared by manufactured sand: mechanical strength and micro structure, Constr. Build. Mater. 452 (2024) 139001.
[16] E. Masad, D. Olcott, T. White, L. Tashman, *correlation of imaging shape indices of fine aggregate with asphalt mixture performance*. Proc., 80th annual meeting of, Transp. Res. Board Wash. D. C. Pap. No. 012123. (2001).
[17] MathWorks, *matlab, version r2023a* [Computer software], The MathWorks, Inc., Natick, MA, 2023. ⟨https://www.mathworks.com⟩.
[18] S. Pyo, S. El-Tawil, Capturing the strain hardening and softening responses of cementitious composites subjected to impact loading, Constr. Build. Mater. 81 (2015) 276–283.
[19] S. Pyo, K. Wille, S. El-Tawil, A.E. Naaman, Strain rate dependent properties of ultra high performance fiber reinforced concrete (UHP-FRC) under tension, Cem. Concr. Compos. 56 (2015) 15–24.
[20] M.A. Saqif, S. El-Tawil, "Characterization of the tension softening behavior of UHPC, Constr. Build. Mater. 409 (2023) 134063.
[21] C.A. Schneider, W.S. Rasband, K.W. Eliceiri, NIH image to ImageJ: 25 years of image analysis, Nat. Methods 9 (7) (2012) 671–675.
[22] D. Su, W.M. Yan, "Quantification of angularity of general-shape particles by using Fourier series and a gradient-based approach.", Constr. Build. Mater. 161 (2018) 547–554.
[23] K. Wille, A.E. Naaman, S. El-Tawil, G.J. Parra-Montesinos, Ultra-high performance concrete and fiber reinforced concrete: achieving strength and ductility without heat curing, Mater. Struct. 45 (2012) 309–324.
[24] K. Wille, A.E. Naaman, Pullout behavior of High-Strength steel fibers embedded in Ultra-High-Performance concrete, Acids Mater. J. 109 (4) (2012).
[25] R. Yang, R. Yu, Z. Shui, C. Guo, S. Wu, X. Gao, S. Peng, The physical and chemical impact of manufactured sand as a partial replacement material in Ultra-High performance concrete (UHPC), Cem. Concr. Compos. 99 (2019) 203–213.